Quantum Mechanics Calculations on Rhodamine Dyes Require Inclusion of Solvent Water for Accurate Representation of the Structure

Luigi Cavallo,[‡] Madeleine H. Moore,[§] John E. T. Corrie,[†] and Franca Fraternali*[,†]

National Institute for Medical Research, The Ridgeway, Mill Hill, London, NW7 1AA, United Kingdom, University of Salerno, Department of Chemistry, via Salvador Allende, I-84081 Baronissi (SA), Italy, and York Structural Biology Laboratory, Department of Chemistry, University of York, Heslington, York YO1 5DD, United Kingdom

Received: May 18, 2004

DFT studies of structural and electrostatic properties of two rhodamines are reported. For one compound, a sulforhodamine, a crystallographic structure determination was used to validate the computational approach. For the other compound, *N*,*N*,*N*′,*N*′-tetramethylrhodamine, we considered both its lactone and quinonoid forms. Geometry optimization of the quinonoid form required inclusion of solvent effects to prevent its collapse into the lactone. Best agreement with the experimental preference for the quinonoid form in solvents of high polarity was obtained when explicit water molecules were added to a continuous solvent model. The quinonoid structures of both rhodamines are rather rigid molecules, with a strong charge separation mostly localized around the N atoms (positive pole) and around the sulfonate or carboxylate groups (negative pole). In the quinonoid structures, rotation around the N−C(xanthene) bond is considerably restricted by extensive conjugation of the N atoms with the xanthene ring. The lactone form is characterized by reduced charge separation and a much lower barrier for the rotation around the N−C(xanthene) bond. The calculated energy barrier for the interconversion between the quinonoid and lactone forms is low, in good agreement with the experimentally observed easy interconversion between the two forms.

Introduction

Rhodamine fluorophores find wide utility in biological research because of their brightness and relative resistance to photobleaching. Most applications in this context involve covalent attachment of the dye to a biomolecule to enable its observation by some form of fluorescence microscopy, and range from qualitative localization studies to detailed biophysical measurements. In the latter context, one such method that has been applied to obtain information on the orientation and motion of protein domains within their native cellular environment uses fluorescence polarization measurements on proteins labeled at two cysteine residues with the bifunctional rhodamine **1**.[1] Two-point attachment of the fluorophore aims to restrict its independent motion, so its orientation within a reference frame, determined from fluorescence polarization data, reports the orientation to the protein domain to which it is attached.[2−6] In this method, the mean probe orientation with respect to the protein is assumed on average to lie with the long axis of the xanthene ring system parallel to the line that joins the β-carbons of the labeled cysteines. This axis of the xanthene is collinear with the fluorescence dipole.[7] An NMR structural study of the N-terminal lobe of troponin C, labeled with **1** on its C helix, confirmed that the native structure was not perturbed by the label but was unable directly to determine the orientation distribution of the label because of the absence of NOE contacts between the label and the protein.[8]

An alternate approach to determining the orientation and dynamics of this rhodamine probe attached to a protein would be by molecular dynamics simulations, but implementing this requires detailed knowledge of the structural and electronic charge properties of the rhodamine. We were unable to find an appropriate theoretical description of these dyes and therefore undertook a computational study of two different rhodamines. The first, sulforhodamine **2**, was chosen because it was suitable for X-ray crystallography and the resultant structural coordinates were therefore available to validate the computational approach. Crystallographic details are given in the Supporting Information. The second compound was a simplified analogue of **1**, namely *N*,*N*,*N*′,*N*′-tetramethylrhodamine **3**, for which it was necessary to consider the lactone and quinonoid forms, hereafter labeled as **3-l** and **3-q** respectively. As discussed below, inclusion of solvent effects was essential to describe the equilibrium between the two isomers of **3**, since in the gas phase we were unable to locate a geometry corresponding to the quinonoid **3-q** form. Thus, while gas-phase geometry optimizations were adequate for **2**, in the case of **3** we considered two different solvent models. First we simply included a continuous aqueous solvent but subsequently improved this model by inserting two explicit water molecules.

SCHEME 1

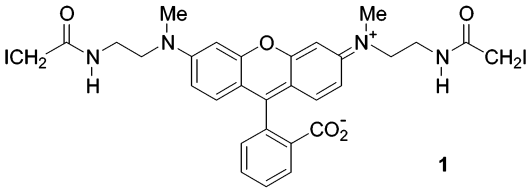

1

The greater tendency for **3** to lactonize in the gas phase compared to **2** is in line with the higher nucleophilicity of the carboxylate anion. It is also compatible with experimental data that the lactone (colorless) form is favored when rhodamines

* To whom the correspondence should be addressed: E-mail: ffranca@nimr.mrc.ac.uk.
[†] National Institute for Medical Research.
[‡] University of Salerno.
[§] University of York.

10.1021/jp047863p CCC: $27.50
Published on Web 08/26/2004

CHART 1: Structures of Rhodamines Studied. Atom Numbers Are Used in the Text to Define Structural Parameters. Torsion Angle σ_1 Is Defined by the Sequence C12−C11−C9−C8′, while the Torsion Angles σ_2 and σ_2' Are Defined by the Sequences C2−C3−N13−C14 and C7−C6−N16−C17, Respectively

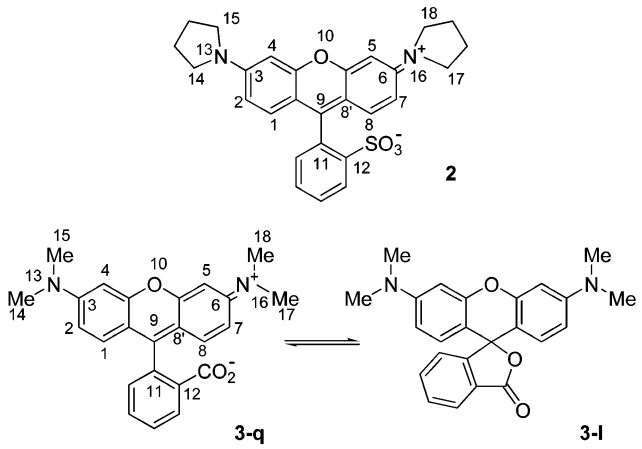

such as **3** are dissolved in a nonpolar solvent and that the equilibrium shifts toward the quinonoid (colored) form as the polarity of the solvent is increased.[9−14]

The present paper describes the results of density functional theory (DFT) calculations of the model rhodamines **2** and **3** to shed light on their structure and conformational freedom around the torsion angles σ_1 and σ_2 (defined in Chart 1), and on their electronic and electrostatic properties. Moreover, for **3** we also investigated in detail the relative stability of the quinonoid and lactone forms, and energy barriers for their mutual interconversion. As already mentioned, it was necessary to include both implicit and explicit solvent water to be able to calculate an accurate representation of the rhodamine **3**, the relevant model for the bifunctional rhodamine **1**. Significantly, we will show for the systems here considered that careful attention to solvent effects is mandatory, not only for adequate estimation of relative energies but also for the description of structural aspects.

Computational Details

All DFT calculations were performed at the B3LYP level of theory[15−17] with the Gaussian03 program package.[18] The 6-31G(d,p) basis set[19−21] was used for geometry optimization of all systems. To determine better energy evaluations we performed single-point calculations on all the geometries obtained, using the extended 6-311G(d,p) and 6-311+G(d,p) basis sets.[20,22]

All geometry optimizations and energy calculations for **2** were performed in the gas-phase but different models of the environment were considered for **3**, as we were unable to locate a geometry corresponding to **3-q** in the gas-phase despite trying several different strategies to locate it. These included (i) improving the basis set to 6-31+G(d,p) to include diffuse functions that should stabilize the anionic carboxylate group,[23] (ii) performing preliminary constrained geometry optimizations with the plane of the carboxylate group fixed perpendicular to the phenyl ring, and (iii) starting from several different geometries. However, when the system was fully relaxed the final gas-phase geometry after energy minimization was always the lactone **3-l**, independent of the basis set used.

The first aqueous solvent for **3** was modeled as a continuum medium with the PCM model of Tomasi.[24−26] In the second model, in addition to the continuum medium modeled with PCM we inserted two explicit water molecules near the carboxylate group. We refer to the systems in the presence of these two explicit water molecules as **3-q/2w** and **3-l/2w**. To optimize the positions of the two added water molecules, we performed several test calculations with randomly chosen geometries for the water molecules. To save computer time, these test calculations used the smaller 3-21G basis set[27] with the Gaussian keyword "*Loose*" to define lower convergence criteria. The best three geometries for both **3-l/2w** and **3-q/2w**, all within 2 kcal/mol, were then refined with the 6-31G(d,p) basis set and standard Gaussian convergence criteria. After this refinement, we obtained the same order of energies as with the 3-21G basis set. In all cases the most stable geometries are found when each oxygen of the CO_2^- group is paired via a hydrogen bond to a partner water molecule, while a further hydrogen-bonded interaction is established between the two water molecules. This maximizes the number of hydrogen bonds that can be formed. Thus, the small energy differences we calculated are a consequence of slightly different conformational arrangements of the water molecules which, of course, lie on rather shallow energy minima. Although we cannot prove that we located the global minimum energy geometries, the fact that the majority of the geometries we tested converged into similar minima or into a family of structures with substantially similar energy suggests the strategy is accurate enough to provide reliable and useful results.

The interconversion reaction between these two forms was modeled only in the presence of the explicit water molecules. The transition state that connects **3-q/2w** and **3-l/2w** was approached with a linear transit procedure from **3-q/2w**, using the developing C(xanthene)−O bond as the reaction coordinate. The step size was 0.05 Å. To test the linear transit path traced in this way, we scanned the chosen reaction coordinate backward from **3-l/2w**, using a coarser step of 0.1 Å. The real transition state search was started from the geometry corresponding to the maximum of the linear transit path. The nature of the transition state was confirmed with frequency calculations that resulted in only one negative vibrational mode.

Natural Bond Order (NBO) analysis[28] was used extensively in rationalizing the results. Beside the NBO index, we used charges derived from Natural Population Analysis (NPA)[28] when rationalizing charge localization. We prefer the NPA charges to standard Mulliken charges because the latter have a strong dependence on the chosen basis set, particularly when diffuse functions are used. In contrast, NPA charges are essentially independent of the basis set.[29]

Finally, to validate our computational approach, we compared the B3LYP energy barrier for rotation around the N−C(aromatic) bond in model systems of aniline **4** and *N*,*N*-dimethylaniline **5**, with the barrier calculated at the coupled cluster with single and double excitations with the perturbatively connected excitations approach, CCSD(T), and the top level post-scf approach.[30,31]

Results and Discussion

Optimized Structure for Sulforhodamine 2: Testing the Computational Approach. The X-ray structure of **2** is shown in the Supporting Information and, to our knowledge, is the only structure of a rhodamine alone. Other published structures contain complexed metals (Rh or Pt) in addition to the fluorophore.[32,33] In our structure the rhodamine is present in a face-to-face dimer and (per rhodamine monomer) contains a molecule each of water and methanol, mutually hydrogen-bonded, within the unit cell together with partial occupancy by a second water molecule. These solvent molecules in the unit cell are located far from the rhodamine and are unlikely to significantly perturb its structure.

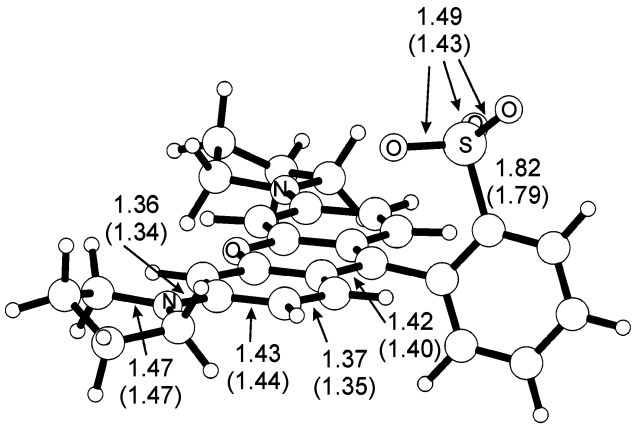

Figure 1. Optimized geometry and selected geometrical parameters for **2**. Values in parentheses refer to the X-ray structure. Distances in Å.

The optimized calculated geometry of **2** is shown in Figure 1. The overall agreement with the X-ray structure is demonstrated by the good agreement of calculated and experimental distances illustrated in the figure and of the calculated and experimental values of the torsion angles σ_1, σ_2, and $\sigma_{2'}$, with the calculated values being on average within 3° of the experimental values. A complete listing of optimized coordinates is given in the Supporting Information. The main differences from the crystallographic structure involve the sulfur atom, where values for bonds are systematically longer in the calculated geometry, and the C(xanthene)−C(phenyl) bond that bends out of the mean xanthene plane by only 2° in the X-ray structure but by 8° in the calculated geometry. This angle in the crystal structure may be affected by the partner rhodamine in the dimer but we have not attempted to investigate this point.

As expected, the two N atoms are strongly conjugated to the xanthene skeleton, consistent with N−C(xanthene) bonds (1.36 Å) that are considerably shorter than the N−C(pyrrolidine) bonds (1.47 Å). However, this difference in the N−C bond lengths is not conclusive of participation by the N atom in the conjugated system, since the xanthene and pyrrolidine carbon atoms are in different hybridization states. Clearer evidence is found in (i) the substantially planar geometry around the N atoms (which are only 0.02 Å out of the plane defined by the three C atoms directly bonded to the them), consistent with sp^2 hybridization of the N atoms, and (ii) the NBO index of the N−C(xanthene) bonds, 1.20 (significantly greater than 1, that would correspond to a single σ-bond). The 1.20 value is very close to the NBO of C2−C3 (1.23) and slightly lower than the NBO of the C7−C8 bond (1.32) (see Chart 1 for the atom numbering scheme). In comparison, the NBO of the N−C(pyrrolidine) bonds is 0.96. These values are consistent with participation of the N atoms in the conjugated framework.

With regard to conformational freedom around the torsion angles σ_1 and σ_2, Table 1 reports the energy of four structures separately optimized with the constraint that torsion angles σ_1 or σ_2 were fixed at 0° or at 90°. Beside the single constraint on σ_1 or σ_2, all other degrees of freedom (including $\sigma_{2'}$) were completely relaxed for each optimization. Energy differences are calculated relative to the fully optimized structure of Figure 1. Notably, the data indicate that the magnitudes of barriers around σ_1 and σ_2 are scarcely affected by the quality of the basis set.

The calculations suggest that rotation to $\sigma_1 = 90°$ is easily accessible, which is expected since the minimized value of σ_1 deviates by only ~5° from 90° (Figure 1). The geometry with $\sigma_1 = 0°$ is much higher in energy and a barrier of about 27 kcal/mol is calculated for rotation to this angle. These findings are broadly compatible with similar results for substituted biphenyls.[34,35] For example, in 2,2′-dichlorobiphenyls, the inter-ring torsion angle (analogous to σ_1) is calculated to be close to 85° in the minimum energy conformation, and conformations with the torsion angle equal to 180° and 90° are about 20 kcal/mol and <0.1 kcal/mol respectively higher in energy. Note that in this case the 180° torsion angle corresponds to a planar conformation (i.e., analogous to $\sigma_1 = 0°$) in which the two chlorines are in a *trans* relationship. When the two chlorines are *cis* (i.e., the torsion angle is 0°), the energy is much higher because of severe steric interactions between the *ortho*-substituents.[34,35]

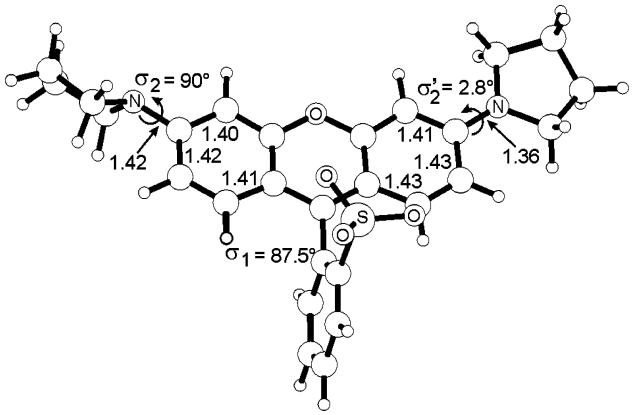

Figure 2. Optimized geometry and some geometrical parameters (distances in Å) for **2** with the dihedral angle σ_2 around the N13−C3 bond fixed at 90°.

TABLE 1: Energy Differences (ΔE, kcal/mol), for 2 with the Torsion Angles σ_1 or σ_2 Fixed at 0° and 90°, Relative to the Fully Relaxed Geometry of Figure 1

basis set	$\sigma_1 = 0°$	$\sigma_1 = 90°$	$\sigma_2 = 0°$	$\sigma_2 = 90°$
6-31G(d,p)	26.5	0.2	0.1	11.5
6-311G(d,p)	27.0	0.1	0.1	11.6
6-311+G(d,p)	27.6	0.2	0.1	11.4

The minimized value of σ_2 deviates by only 4° from 0° and our calculations indicate that rotation to $\sigma_2 = 0°$ is easily accessible. In contrast, a substantial barrier, ~11.5 kcal/mol, was found for the geometry with $\sigma_2 = 90°$ and the corresponding structure is shown in Figure 2. The barrier around σ_2 arises principally from disruption of conjugation between the xanthene ring and the N13 atom. This loss of conjugation upon rotation to $\sigma_2 = 90°$ would be expected and is supported by the following aspects of the calculations: (i) in the geometry with $\sigma_2 = 90°$ the N13 atom is strongly sp^3 hybridized, as indicated by the substantial pyramidal geometry it assumes, with the N13 atom 0.39 Å out of the plane defined by the three C atoms bonded to it; (ii) the N13−C(xanthene) bond is substantially elongated (by 0.06 Å) relative to the fully relaxed geometry; (iii) the NBO of the N13−C(xanthene) bond is reduced by 0.17 relative to the fully relaxed geometry to 1.03, which is indicative of a single σ-bond. The nature of the other N−C(xanthene) bond (N16−C6), involving the pyrrolidine that does not rotate out of the xanthene plane, is not substantially altered although there is evidence of marginally higher participation of N16 with the conjugated skeleton, since the N16−C6 bond is calculated to shrink by 0.01 Å and its NBO to increase by 0.02.

Charge Separation in Sulforhodamine 2. To estimate charge separation in **2**, we first partitioned the molecule into two subsystems, one composed by the SO_3^--substituted phenyl

ring and the second composed by all of the other atoms, namely those of the xanthene skeleton and the two pyrrolidine rings. The charge analysis is based on the NPA approach, as described in Computational Details. On summing the 6-31G(d,p) NPA charges of the atoms within the two subsystems, the sulfonated aromatic moiety has a total charge of −0.84 e while the other part, as expected for a molecule with no net charge, has a total charge of +0.84 e. For a more detailed analysis of charge localization, we calculated by the same means the charge of the SO_3^- group only (−0.53 e) and the charge of the substructures that comprise the N atoms together with the C(xanthene) atom and CH_2(pyrrolidine) groups directly bonded to them. The total charge of the latter units is +0.48 e, so each of the N-based units has a total charge of +0.24 e. The analysis therefore indicates strong charge separation within the molecule, with the charges mostly localized on the SO_3^- group and around the N atoms. This net charge localization results in a dipole moment of 15.7 D, which lies substantially in the local C_s symmetry plane perpendicular to the xanthene skeleton and forms an angle of ∼42° with the xanthene plane. In the structure with $\sigma_2 = 90°$, the charge on the unit comprising N13 and the three C atoms bonded to it reduces to only +0.08 e, while that on the unit centered on N16 increases slightly to +0.27 e. The reduced positive charge around N13 in this twisted conformer indicates that charge transfer from the N atoms to the xanthene skeleton occurs through π-conjugated molecular orbitals.

Calculated Structures for Tetramethylrhodamine 3. The good agreement of calculated and experimental structures for **2** validated the computational methods for this system and allowed us to proceed to the tetramethylrhodamine **3**, for which crystallographic data were not available. Optimized geometries of **3-q/2w** and **3-l/2w** are shown in Figure 3. Formation of the C9−O bond naturally changes the hybridization of C9 from sp^2 to sp^3. In both **3-q/2w** and **3-q**, the C(xanthene)−C(phenyl) bond bends out of the mean xanthene plane by ∼7°. However, in the light of the previous comparison between calculated and crystallographic geometries of **2**, the extent of this distortion is probably overestimated. As found for **2**, the torsion angles σ_1, σ_2, and $\sigma_{2'}$ assume values very close to 90°, 0° and 0°, respectively. Small differences between **2** and **3-q/2w** on the one hand, and **3-l/2w** on the other hand, are found in the geometry of the N atoms. In **2** and **3-q/2w** the N atoms are essentially in the plane defined by the three C atoms bonded to them (the out-of-plane displacement of the N is only 0.02 Å) but for **3-l/2w** there is a slight pyramidalization of the N atoms, indicated by their larger out-of-plane displacement of 0.08 Å. This finding, combined with slightly longer N−C(xanthene) bonds in **3-l/2w** (0.02 Å longer relative to **3-q/2w**), suggests reduced conjugation of the N atoms with the xanthene skeleton in **3-l/2w**. This is expected as the xanthene no longer bears a formal positive charge and reduced conjugation is confirmed by the NBOs of the N−C(xanthene) bonds, which are 1.24 in **3-q/2w** but only 1.17 in **3-l/2w**. Very similar differences are also observed in the absence of the two explicit water molecules.

In both **3-q/2w** and **3-l/2w**, each oxygen atom of the carboxylate group forms one hydrogen bond, each with a separate water molecule: the two water molecules also interact with each other through a hydrogen bond. This gives rise to a hydrogen-bonded cyclic structure. The water−water hydrogen bond distance is in line with values we calculated with the same basis set for the isolated, gas-phase water dimer, suggesting that geometries for the cyclic structures involving the water molecules are substantially unstrained. We found somewhat different orientations for the two water molecules in **3-l/2w** and **3-q/2w**.

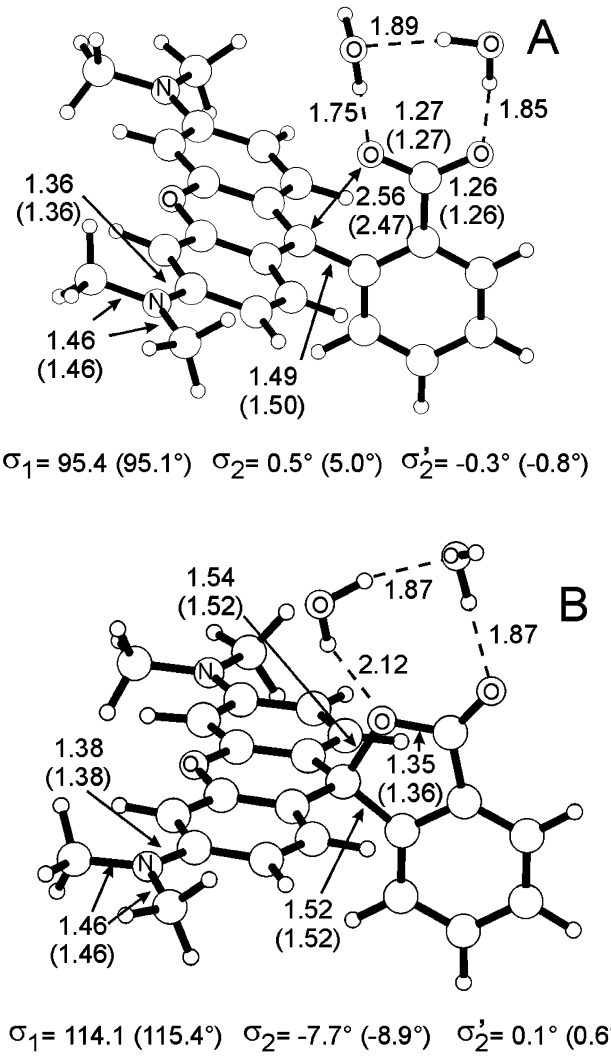

Figure 3. Optimized geometries and selected geometrical parameters for the **3-q/2w** (panel A) and **3-l/2w** (panel B) systems. Values in parentheses refer to the **3-q** and **3-l** systems. Distances are in Å.

However, in solution the rearrangement of water molecules is expected to be sufficiently rapid that the most stable calculated structures can always be compared, independently of small differences in orientation of the two water molecules.

Finally, while the **3-l** and **3-l/2w** geometries are extremely similar, the C9−O distance in **3-q** is ∼0.1 Å shorter than in **3-q/2w**. The specific effect of the two water molecules in **3-q/2w** that stabilize the carboxylate group illustrates the need for careful treatment of solvent effects to obtain a satisfactory description of this system.

The energy differences between **3-q** and **3-l**, ΔE_{q-l}, and **3-q/2w** and **3-l/2w**, $\Delta E_{q/2w-l/2w}$, are reported in Table 2. Negative ΔE values are found when the quinonoid form is energetically favored. In the gas-phase **3-l** is substantially more stable than **3-q** (entry 1). Inclusion of a continuous aqueous solvent stabilizes **3-q** relative to the gas-phase by 15.8 kcal/mol (entry 2) and this stabilization is further enhanced with the more-extended 6-311G(d,p) basis set (entry 3). When diffuse functions are included there is an inversion of stability and **3-q** becomes favored over **3-l** (entry 4). Thus polar solvents stabilize the quinonoid form. Addition of two explicit water molecules to the model gives additional stability to the quinonoid form but in the gas phase the effect is insufficient to make **3-q/2w** more stable than **3-l/2w** (entry 5). However, in combination with the continuous solvent the two explicit waters are sufficient to invert

TABLE 2: B3LYP Energy Differences, ΔE_{q-l} and $\Delta E_{q/2w-l/2w}$, (kcal/mol)

entry	system	medium	basis set	$\Delta E_{quinonoid-lactone}$
1[a]	isolated **3**	gas phase	6-31G(d,p)	20.4
2	isolated **3**	implicit water	6-31G(d,p)	4.6
3[a]	isolated **3**	implicit water	6-311G(d,p)	2.4
4[a]	isolated **3**	implicit water	6-311+G(d,p)	−1.9
5[b]	**3** + 2 explicit waters	gas phase	6-31G(d,p)	12.7
6	**3** + 2 explicit waters	implicit water	6-31G(d,p)	−2.2
7[b]	**3** + 2 explicit waters	implicit water	6-311G(d,p)	−4.0
8[b]	**3** + 2 explicit waters	implicit water	6-311+G(d,p)	−6.3

[a] Geometry of entry 2. [b] Geometry of entry 6.

the order of stability of the two systems and to render **3-q/2w** more stable than **3-l/2w** with all basis sets. As is the case in the absence of the two explicit water molecules, more extended basis sets stabilize **3-q/2w** more than **3-l/2w** (entries 6 and 7). With the more extended 6-311+G(d,p) basis set, the quinonoid form is significantly more stable than the lactone (entry 8).

To summarize, the relative stability of the two forms depends slightly on the basis set used. More extended basis sets and inclusion of diffuse functions stabilize the quinonoid form. This is a direct consequence of the much more diffuse electron density around the anionic CO_2^- group in the quinonoid form, which is better described with more extended basis sets, particularly with the inclusion of diffuse functions.[23] On the other hand, more extended basis sets and diffuse functions have a smaller influence on the energy of the lactone form, where the anionic CO_2^- group is not present. Much more relevant is the fact that the stability of the quinonoid form is strongly dependent on the dielectric properties of the solvent. Our calculations suggest that, in the gas-phase or in solvents of low polarity, the lactone is more stable than the quinonoid form. In contrast, the quinonoid form is strongly stabilized in protic solvents and specific hydrogen-bond interactions between the anionic CO_2^- group and a protic solvent are a dominant factor in this stabilization. Our results are in good qualitative agreement with spectroscopic data for the interconversion of colorless and colored forms of *N*,*N*′-substituted rhodamines in solutions of different dioxane−water mixtures.[9,10] Related experimental studies show similar effects.[11−14] As the water concentration increases, colorless lactone forms are converted into the colored quinonoid forms. The polarity of the solvent, the microenvironment of the anionic CO_2^- group and the nature of the substituents on the nitrogen atoms all contribute to positioning the equilibrium.

Torsion barriers for **3** were calculated only for rotation about the N−C(xanthene) bond, since the results for **2** had shown that only rotation about this bond was reasonably accessible. Thus, we ran constrained geometry optimizations for **3-q/2w** and **3-l/2w** with σ_2 fixed at 90°. For **3-q/2w** the geometry with $\sigma_2 = 90°$ is 11.9 kcal/mol higher in energy than for the completely relaxed structure. This value is close to the one calculated for **2** and is only slightly affected by the quality of the basis set (see Table 3). As determined for **2**, the N13 atom at $\sigma_2 = 90°$ undergoes a marked change of hybridization compared to the relaxed structure and conjugation with the aromatic skeleton is lost: the NBO of the N13−C(xanthene) bond is 1.03, and the N13 atom is 0.40 Å out of the plane defined by the three C atoms bonded to it.

Table 3 also shows data for **3-l/2w**. The geometry with $\sigma_2 = 90°$ is only 5.5 kcal/mol higher in energy than for the relaxed **3-l/2w** structure and more extended basis sets have little effect. As in the quinonoid form, the hybridization of the N13 atom changes considerably from the relaxed structure because of lost conjugation with the aromatic skeleton. The NBO of the N13−C(xanthene) bond is 1.01, and the N13 atom is 0.41 Å out of the plane defined by the three C atoms bonded to it. The lower barrier around σ_2 for **3-l/2w** is consistent with reduced conjugation of the N atoms in **3-l/2w**. In the absence of extended conjugation, the rotational barrier about the N−C(xanthene) bond should be similar to that in simple aromatic amines, such as aniline **4** and its *N*,*N*-dimethyl analogue **5**. We therefore calculated the barrier around the N−C(aromatic) bond in **4** and **5** to validate our computations. For aniline itself we compared the barrier at the B3LYP level with that calculated at the CCSD(T) level. The CCSD(T) calculations were performed on the B3LYP 6-31G(d,p) geometries: to check for the effect of the basis set on convergence of this barrier at the CCSD(T) level we also used the 6-31G(d,p), 6-311G(d,p), and 6-311+G(d,p) basis sets. For *N*,*N*-dimethylaniline **5** we calculated the barrier at the B3LYP level only.

TABLE 3: Energy Barriers (kcal/mol) for Rotation around the Torsion Angle σ_2 for 3-q/2w, 3-l/2w, 4, and 5, and for the Conversion of 3-q/2w into 3-l/2w

barrier	6-31G(d,p)	6-311G(d,p)	6-311+G(d,p)
around σ_2 for **3-q/2w**	11.9	11.8	12.4
around σ_2 for **3-l/2w**	5.5	5.1	4.9
around σ_2 for **4**[a]	5.7		
around σ_2 for **4**[b]	3.9	3.7	3.9
around σ_2 for **5**[a]	3.7		
3-q/2w → **3-l/2w**	4.3	5.2	6.8

[a] B3LYP barrier. [b] CCSD(T) barrier (see the Computational Details Section).

The CCSD(T) barriers for **4** are 3.9, 3.7, and 3.9 kcal/mol with the 6-31G(d,p), 6-311G(d,p), and 6-311+G(d,p) basis sets, indicating that the CCSD(T) barrier is not dependent on the basis set. The B3LYP barrier, 5.7 kcal/mol, overestimates the CCSD(T) barrier by roughly 2 kcal/mol, which gives an idea of the level of error in the present calculations. The B3LYP barrier for **5**, 3.7 kcal/mol, is about 2 kcal/mol lower than the corresponding barrier for **4** and is probably connected to steric repulsion between the methyl groups and the *ortho*-hydrogens. The barrier we calculated for **3-l/2w** is in good agreement with the barrier for **5**, indicating that the much lower barrier in **3-l/2w** relative to **3-q/2w** reflects the reduced conjugation in the lactone. Finally, the barrier we calculated for **5** is in reasonable agreement with the ΔG value of 5.1 ± 1.0 kcal/mol estimated for the same rotation in this compound from dynamic NMR studies of several substituted *N*,*N*-dimethylanilines in low-polarity organic solvent.[36]

Charge Separation in Tetramethylrhodamine 3. Estimation of charge separation in **3-q/2w** followed the protocol described for **2**; that is, we first partitioned the molecule into two subsystems, one comprising the CO_2^--substituted aromatic ring and the second comprising all remaining atoms of the xanthene moiety and the two dimethylamino groups. We then summed the 6-31G(d,p) NPA charges of atoms belonging to the two subsystems. The CO_2^--substituted aromatic ring has a total

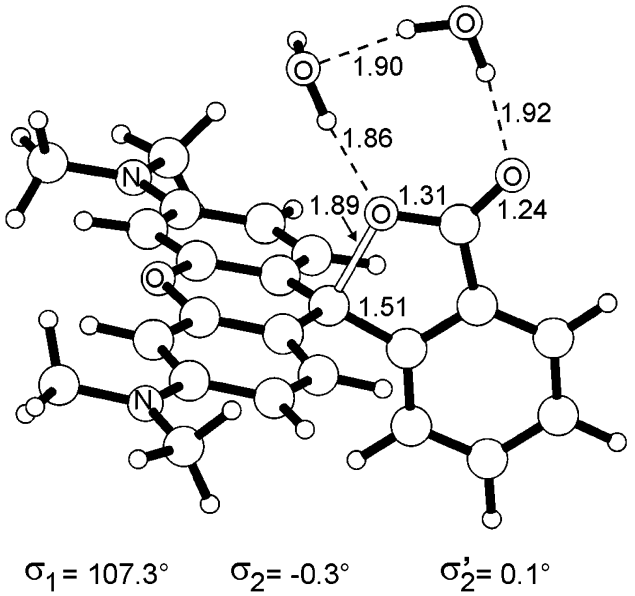

Figure 4. Transition state for the interconversion between **3-q/2w** and **3-l/2w**.

charge of −0.78 e, while the xanthene skeleton and the two NMe_2 groups have a total charge of +0.89 e. The residual charge of −0.11 e is transferred from the rhodamine to the two water molecules. Further, to quantify the degree of charge localization the same approach was used to calculate the charge of the CO_2^- group alone (−0.71 e) and the charge of the substructures that comprise the NMe_2 groups and the C(xanthene) atoms directly bonded to them. The total charge of the two units is +0.68 e, so each of the N-based groups has a total NPA charge of +0.34 e. This analysis suggests a stronger charge localization for **3-q/2w** than for **2**, which is reasonable as the β-CH_2 groups of the pyrrolidine ring of **2** would allow for inductive delocalization of charge. In fact, the charge of the N−C(xanthene) group increases by 0.04 e on going from **2** to **3-q/2w**.

The net charge localization results in a dipole moment of 19.0 D. As for **2**, the dipole moment lies in the local C_s symmetry plane that is perpendicular to the xanthene skeleton and forms an angle of about 39° with the xanthene plane. Finally, with $\sigma_2 = 90°$ the charge on the NMe_2 group centered on the N13 atom amounts only to +0.12 e, while that on the NMe_2 group centered on the N16 atom, +0.39 e, is slightly larger than in the completely relaxed **3-q/2w**. As for **2**, this indicates that the strong charge localization around the N atoms is a consequence of their conjugation with the xanthene skeleton.

We similarly estimated the charge separation in **3-l/2w**. Of the two subsystems defined as before, the carbonyl-substituted ring has a total charge of −0.36 e while the NMe_2-substituted xanthene has a total charge of +0.42 e, and only −0.06 e is transferred to the two water molecules. The charge calculated for the oxycarbonyl moiety alone is −0.38 e while that of the two NMe_2 groups is +0.42 e. In short, this analysis suggests that charge separation is much reduced in the lactone compared to the quinonoid form, as expected upon abolition of the zwitterionic system in the latter.

Calculation of the Barrier for Interconversion Between 3-q/2w and 3-l/2w. As a final point in the characterization of the quinonoid and lactone forms in solution, we investigated the energy barriers for interconversion of **3-q/2w** and **3-l/2w**. The geometry of the transition state is reported in Figure 4. The developing C−O bond is 1.89 Å long. The carbon−oxygen bonds of the CO_{2-} group become asymmetric; the one evolves toward a carbonyl bond shrinking by 0.02 Å, while the other elongates by 0.04 Å. The negative frequency corresponding to the maximum of the energy along the reaction coordinate is −249 cm^{-1}. At the 6-31G(d,p) level of theory the transition state is 4.3 kcal/mol higher in energy than **3-q/2w**. This value corresponds to the energy barrier for conversion of **3-q/2w** into **3-l/2w**. Increasing the quality of the basis set to 6-311G(d,p) and 6-311+G(d,p) increases this barrier to 5.2 and 6.8 kcal/mol, respectively. From the relative energies of **3-q/2w** and **3-l/2w** (Table 2), the barrier calculated for the reverse reaction, that is, for conversion of **3-l/2w** to **3-q/2w**, is much lower at 2.1, 1.2, and 0.5 kcal/mol with the 6-31G(d,p), 6-311G(d,p) and 6-311+G(d,p) basis sets, respectively. This very low energy barrier raises a question of whether the lactone form is stable in water. However, accurate consideration of this point would require a more refined model for the solvent and more extended basis sets, both of which are computationally prohibitive at present.

Conclusion

In this work we studied the conformational and electrostatic properties of the rhodamines **2** and **3** and validated the computational method by comparison of the calculated and experimental structures of **2**, and by comparison of energy barriers around σ_2 for **3** with high-level CCSD(T) calculations on model anilines. Experimental values are in reasonable agreement with these calculated values. Compound **3** is of particular interest since it presents an equilibrium between ring-chain tautomers corresponding to the colorless lactone, **3-l**, and to the colored quinonoid, **3-q**, forms. This behavior required careful consideration of solvation in order to be able to reproduce experimentally observed data.

2 and **3-q** have one conformational energy minimum with σ_1 close to 90°, and rotation around this angle is strongly disfavored because of steric repulsions between the *ortho*-substituents. The dihedral angle σ_2 is close to 0° and a barrier of about 10 kcal/mol is calculated for rotation around this angle, mainly due to the disruption of the conjugation between the xanthene ring and the N atoms. The σ_2 barrier in the lactone **3-l** is much lower, about 5 kcal/mol. Structural analysis and comparison with model anilines indicate that this lower barrier originates from the absence of the formal positive charge on the xanthene ring in the lactone form, which results in much-reduced conjugation of the N atoms with the aromatic moiety.

Both **2** and **3-q** have strong charge separation and the charges are mostly localized on the SO_3^- or CO_2^- group, for **2** and **3-q**, respectively, and around the N atoms. This net charge localization results in a dipole moment greater than 15 D for **2** and **3-q**: the dipole lies in the local C_s symmetry plane perpendicular to the xanthene skeleton. Thus, rhodamines can be considered as stiff molecules composed of two discoid subunits (the xanthene system and the substituted phenyl ring) nearly perpendicular to each other, with a net charge separation roughly localized as shown in Figure 5.

We also investigated the relationship between the polarity of the solvent and the equilibrium between the colorless lactone and the colored quinonoid forms. In vacuo (which represents the extreme nonpolar solvent) we were unable to detect the quinonoid **3-q** form. Inclusion of an implicit solvation model enables location of both the **3-q** and **3-l** forms. However, the quinonoid form is 2−4 kcal/mol less stable than the lactone form with the 6-31G(d,p) and 6-311G(d,p) basis sets. Only with the 6-311+G(d,p) basis set was the quinonoid **3-q** form calculated to be more stable (by < 2 kcal/mol) than the lactone.

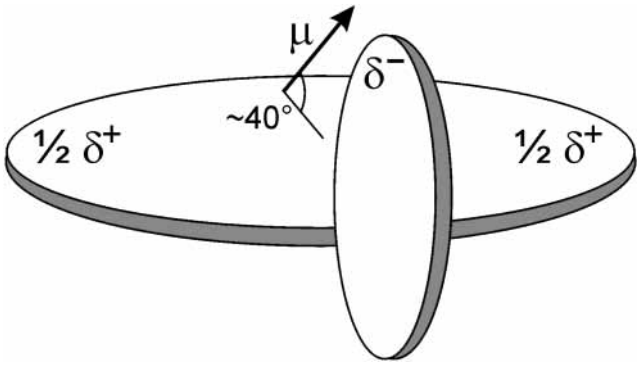

Figure 5. Schematic representation of rhodamines as composed of two discoid subunits nearly perpendicular to each other and with strong charge separation. The 1/2 δ^+ and 1/2 δ^- symbols indicate regions of charge localization. The dipole moment μ arising from this charge separation is represented as an arrow that forms an angle of about 40° with the mean xanthene plane.

These results contrast with the experimental data, which indicate that the equilibrium shifts quantitatively from the lactone to the quinonoid form as the polarity of the solvent increases. To improve the solvation model we added two explicit water molecules. With this approach the quinonoid form is substantially more stable than the lactone form with all the basis sets considered, while it remains significantly less stable than the lactone form in the gas phase. These results well reproduce the experimental behavior. Finally, with the more complex solvent model we investigated the energetics of the reaction that connects the quinonoid and lactone forms. The barrier we calculated for the conversion of **3-q/2w** into **3-l/2w**, about 5 kcal/mol, is in good agreement with the easy interconversion between the colorless and colored forms experimentally observed if the polarity of the solvent is changed.

Our study has shown that an accurate model of the solvent is needed to obtain a representation of real chemical behavior. In fact, although the quinonoid form was favored by 1.9 kcal/mol relative to the lactone with the extended 6-311+G(d,p) basis set and the implicit solvent model, without prior knowledge of the experimental data it would have been clearly difficult to demonstrate whether the stabilization is to be ascribed to solvation or to the particular combination of basis set and implicit water model. Results with the two explicit water molecules are unambiguous, basis-set independent, and conclusive in finding higher relative stability for the quinonoid form.

In conclusion, our experience suggests that in the absence of experimental data, a situation in which computational chemistry is particularly helpful, accurate modeling of the solvent is mandatory to obtain realistic estimates of the energetic and structural properties of the studied systems. Our analysis showed that particular care should be exercised when isomers with different charge separation are possible, such as with neutral and zwitterionic forms of amino acids, or in the case of reactions that present intermediates/transition states with charge separation different from that in reactants and products (see Lilley[37] for a recent review of this possibility in the case of nucleolytic ribozymes).

Acknowledgment. We are grateful to Drs. Zbysek Dauter and Johann Turkenburg, University of York for assistance with crystallographic data. L.C. is indebted to Prof. M. Cossi, University of Napoli, and Dr. G. Scalmani, Gaussian Inc. (formerly of the University of Napoli) for friendly help with the PCM calculations, and Prof. T. K. Woo and the SHARCNET project, University of Western Ontario, for unlimited access to computer resources. Access to facilities of the MRC Biomedical NMR Centre is gratefully acknowledged.

Supporting Information Available: Experimental data for sulforhodamine **2**, Cartesian coordinates and energies of all structures discussed in the paper. A separate cif file gives the crystallographic data for **2**. This material is available free of charge via the Internet at http://pubs.acs.org.

References and Notes

(1) Corrie, J. E. T.; Craik, J. S.; Munasinghe, V. R. N. *Bioconjugate Chem.* **1998**, *9*, 160.
(2) Corrie, J. E. T.; Brandmeier, B.; Ferguson, R. E.; Trentham, D. R.; Kendrik-Jones, J.; Hopkins, S. C.; van der Heide, U. A.; Goldman, Y. E.; Sabido-David, C.; Dale, R. E.; Criddle, S.; Irving, M. *Nature* **1999**, *400*, 425.
(3) Hopkins, S. C.; Sabido-David, C.; van der Heide, U.; Ferguson, R. E.; Brandmeier, B. D.; Dale, R. E.; Kendrick-Jones, J.; Corrie, J. E. T.; Trentham, D. R.; Irving, M.; Goldman, Y. E. *J. Mol. Biol.* **2002**, *318*, 1275.
(4) Ferguson, R. E.; Sun, Y.-B.; Mercier, P.; Brack, A. S.; Sykes, B. D.; Corrie, J. E. T.; Trentham, D. R.; Irving, M. *Mol. Cell.* **2003**, *11*, 865.
(5) Forkey, J. N.; Quinlan, M. E.; Shaw, M. A.; Corrie, J. E. T.; Goldman, Y. E. *Nature* **2003**, *422*, 399.
(6) Peterman, E. J. G.; Sosa, H.; Goldstein, L. S. B.; Moerner, W. E. *Biophys. J.* **2001**, *81*, 2851.
(7) Penzkofer, A.; Wiedmann, J. *Opt. Commun.* **1980**, *35*, 81.
(8) Mercier, P.; Ferguson, R. E.; Irving, M.; Corrie, J. E. T.; Trentham, D. R.; Sykes, B. D. *Biochemistry* **2003**, *42*, 4333.
(9) Ioffe, I. S.; Otten, V. F. *J. Org. Chem. USSR* **1965**, *1*, 333.
(10) Ioffe, I. S.; Shapiro, A. L. *J. Org. Chem. USSR* **1972**, *8*, 1765.
(11) Hinckley, D. A.; Seybold, P. G.; Borris, D. P. *Spectrochim. Acta* **1986**, *42A*, 747.
(12) Hinckley, D. A.; Seybold, P. G. *Spectrochim. Acta* **1988**, *44A*, 1053.
(13) Karpiuk, J.; Grabowski, Z. R.; De Schryver, F. C. *J. Phys. Chem.* **1994**, *98*, 3247.
(14) Mchedlov-Petrossyan, N. O.; Kukhtik, V. I.; Bezguily, V. D. *J. Phys. Org. Chem.* **2003**, *16*, 380.
(15) Becke, A. D. *J. Chem. Phys.* **1993**, *98*, 5648.
(16) Lee, C.; Yang, W.; Parr, R. G. *Phys. Rev. B* **1988**, *37*, 785.
(17) Stephens, P. J.; Devlin, F. J.; Chabalowski, C. F.; Frisch, M. J. *J. Phys. Chem.* **1994**, *98*, 11623.
(18) Frisch, M. J.; Trucks, G. W.; Schlegel, H. B.; Scuseria, G. E.; Robb, M. A.; Cheeseman, J. R.; Montgomery, J. A.; Vreven, T.; Kudin, K. N.; Burant, J. C.; Millam, J. M.; Iyengar, S. S.; Tomasi, J.; Barone, V.; Mennucci, B.; Cossi, M.; Scalmani, G.; Rega, N.; Petersson, G. A.; Nakatsuji, H.; Hada, M.; Ehara, M.; Toyota, K.; Fukuda, R.; Hasegawa, J.; Ishida, M.; Nakajima, T.; Honda, Y.; Kitao, O.; Nakai, H.; Klene, M.; Li, X.; Knox, J. E.; Hratchian, H. P.; Cross, J. B.; Adamo, C.; Jaramillo, J.; Gomperts, R.; Stratmann, R. E.; Yazyev, O.; Austin, A. J.; Cammi, R.; Pomelli, C.; Ochterski, J. W.; Ayala, P. Y.; Morokuma, K.; Voth, G. A.; Salvador, P.; Dannenberg, J. J.; Zakrzewski, V. G.; Dapprich, S.; Daniels, A. D.; Strain, M. C.; Farkas, O.; Malick, D. K.; Rabuck, A. D.; Raghavachari, K.; Foresman, J. B.; Ortiz, J. V.; Cui, Q.; Baboul, A. G.; Clifford, S.; Cioslowski, J.; Stefanov, B. B.; Liu, G.; Liashenko, A.; Piskorz, P.; Komaromi, I.; Martin, R. L.; Fox, D. J.; Keith, T.; Al-Laham, M. A.; Peng, C. Y.; Nanayakkara, A.; Challacombe, M.; Gill, P. M. W.; Johnson, B.; Chen, W.; Wong, M. W.; Gonzalez, C.; Pople, J. A. *Gaussian 03*; Gaussian, Inc.: Pittsburgh, PA, 2003.
(19) Ditchfield, R.; Hehre, W. J.; Pople, J. A. *J. Chem. Phys.* **1971**, *54*, 724.
(20) Gordon, M. S. *Chem. Phys. Lett.* **1980**, *76*, 163.
(21) Hariharan, P. C.; Pople, J. A. *Theor. Chim. Acta* **1973**, *28*, 213.
(22) Krishnan, R.; Binkley, J. S.; Seeger, R.; Pople, J. A. *J. Chem. Phys.* **1980**, *72*, 650.
(23) Hehre, W. J.; Radom, L.; Schleyer, P. v. R.; Pople, J. A. *Ab Initio Molecular Orbital Theory*; John Wiley & Sons: New York, 1986.
(24) Miertus, S.; Scrocco, E.; Tomasi, J. *J. Chem. Phys.* **1981**, *55*, 117.
(25) Tomasi, J.; Persico, M. *Chem. Rev.* **1994**, *94*, 2027.
(26) Cossi, M.; Barone, V.; Cammi, R.; Tomasi, J. *Chem. Phys. Lett.* **1996**, *255*, 327.
(27) Binkley, J. S.; Pople, J. A.; Hehre, W. J. *J. Am. Chem. Soc.* **1980**, *102*, 939.
(28) Reed, A. E.; Curtiss, L. A.; Weinhold, F. *Chem. Rev.* **1988**, *88*, 899.
(29) Wiberg, K. B.; Rablen, P. R. *J. Comput. Chem.* **1993**, *14*, 1504.
(30) Purvis, G. D.; Bartlett, R. J. *J. Chem. Phys.* **1982**, *76*, 1910.
(31) Raghavachari, K.; Trucks, G. W.; Pople, J. A.; Head-Gordon, M. *Chem. Phys. Lett.* **1989**, *157*, 479.
(32) Abrams, M. J.; Picker, D. H.; Fackler, P. H.; Lock, C. J. L.; Howard-Lock, H. E.; Faggiani, R.; Teicher, B. A.; Richmond, R. C. *Inorg. Chem.* **1986**, *25*, 3980.
(33) Thorn, D. L.; Fultz, W. C. *J. Phys. Chem.* **1989**, *93*, 1234.

(34) Arulmozhiraja, S.; Selvin, P. C.; Fujii, T. *J. Phys. Chem. A* **2002**, *106*, 1765.
(35) Grein, F. *J. Phys. Chem. A* **2002**, *106*, 3823.
(36) Mackenzie, R. K.; MacNicol, D. D. *J. Chem. Soc., Chem. Commun.* **1970**, 1299.
(37) Lilley, D. M. J. *Trends Biochem. Sci.* **2003**, *28*, 495.